Supporting Information

Rei et al. 10.1073/pnas.1415845112

SI Experimental Procedures

Animals and RFS Paradigm. Adult male Swiss Webster mice were used at age of 3 mo for the RFS treatment, 10 wk for the BLA and Gi-DREADD cell body viral injections, and 8 wk for the BLA terminal viral injections. For the RFS, Gi-DREADD, and optogenetic experiments, mice were placed in fear-conditioning chambers (TSE Systems). Freezing and behavioral activity were automatically measured on day 4 of the procedure (RFS, RFS/Gi-DREADD, or optogenetic experiments), using the provided fear-conditioning software. For the RFS treatment, mice received 10 foot shocks at an intensity of 0.8 mA and at random intervals during a 1-h session. Control mice were placed in the chamber but did not receive foot shocks. RFS treatment and optogenetic stimulations were repeated once daily for 8 consecutive days. Mice used in immunohistochemistry analyses were killed 90 min after the end of the procedure, and those used in Western blot analyses were killed 20 min after the procedure.

Behavioral Assays. The behavioral arenas consisted of four rectangular rat cages with no bedding, arranged in a 2 × 2 rectangle, separated by four opaque walls. A triangle or three vertical lines of red labeling tape was placed onto the two opposing short walls for spatial cues. For novel object recognition and novel location recognition, special care was taken in habituating the animals to the behavioral arena (10 min per day for 3 d on day 5, 6, and 7 of the RFS) before beginning the object training. On day 7, after the last habituation phase, the novel object location protocol started with the training phase, in which two objects were placed along one short side of each arena (100-mL Pyrex glass bottles, positioned in the corners, 3 cm away from the walls). The mice were placed facing the middle of the opposite short wall at its midsection.

The mice were allowed to familiarize themselves with the objects for two 10-min training sessions, separated by an intertrial interval of 1 h. At 1 h after the second training session, the testing session for the novel location task started; one of the objects was moved to the opposite corner, and the mice were again placed into the arenas. Immediately after this testing period, the novel object recognition procedure started with the training phase, in which the two objects were placed in their original location and the mice were allowed 10 additional min of free exploration. Then 24 h later, one of the glass bottles was substituted for a plastic 55-mL bottle, and the mice were again placed into the arena. For both tests, the time spent with each object (old and new locations or old and new objects) was recorded during a 5-min testing period. During each step of the training and testing, video recordings of the performing mice were acquired using a Sony camcorder fixed to the ceiling above the arenas. Videos were analyzed by an experimenter blinded to the experimental treatment. Mice were scored as exploring an object if they showed obvious signs of directed attention (i.e., sniffing or prolonged observation). Time spent on top of the objects was not counted, unless the mice were simultaneously directing attention to the object. The discrimination index was calculated by dividing the time spent exploring the object with a new component (new object or new location) divided by the sum of the time exploring both objects.

Western Blot Analysis. Western blots were prepared as described previously (1) with the following modifications: proteins were extracted using 1× RIPA buffer containing proteinase (Complete; Roche) and phosphatase inhibitors (1 mM β-glycerophosphate, 10 mM NaF, and 0.1 mM Na_3VO_4), transferred onto PVDF membranes (Bio-Rad), and stripped using stripping buffer (Thermo Scientific). The following primary antibodies were used: rabbit antibody against the C-terminal part of p35 (L.-H. Tsai's laboratory) to detect p35 and p25 proteins, mouse HDAC2 (Abcam), Synaptophysin (Sigma-Aldrich), and β-tubulin and β-actin (Sigma-Aldrich). Secondary antibodies were horseradish peroxidase-linked (GE Healthcare).

Immunohistochemistry. Immunohistochemistry was performed as described previously (1). Analyses under different experimental conditions were performed with the same antibody solution at the same time to ensure identical staining conditions. A negative (i.e., no primary antibody) control was included simultaneously. In brief, mice under deep anesthesia (ketamine, xylazine) were perfused with freshly prepared 4% (wt/vol) paraformaldehyde in PBS, and their brains were sectioned at 40-μm thickness using a vibratome (Leica). Slices were permeabilized with 0.1% Triton X-100, blocked, and incubated overnight with 0.1% Triton X-100/10% donkey serum in PBS containing the following primary antibodies: rabbit HDAC2 (Abcam), mouse Synaptophysin (Sigma-Aldrich), and rabbit c-fos (Santa Cruz Biotechnology). All antibodies were used at 1:1,000 dilution. Primary antibodies were visualized with Alexa Fluor 488 and Cy3 and Cy5 antibodies (Molecular Probes), and neuronal nuclei were visualized with Hoechst 33342 (Invitrogen). Images were acquired using a confocal microscope (LSM 510; Zeiss) at identical settings and focal plan for each condition.

Images were quantified using ImageJ 1.42q. For HDAC2, GR, and pGR quantification and under each experimental condition, three sections (at −1.70, 1.90, and 2.06 mm according to the bregma) were selected, and three images were acquired per section and per hemibrain. In each picture, 40–60 representative cells were analyzed by an experimenter blinded to the experimental treatment, and the mean signal intensity was measured. For Synaptophysin quantification, the same method was used to generate images. Using ImageJ, the stratum radiatum region of the CA1 subfield was selected in each picture, and the mean intensity was quantified.

qRT-PCR. Total RNA was isolated using the PureLink miRNA Isolation Kit (Invitrogen). RNA quantity and quality were measured with a NanoDrop spectrometer. Reverse transcription was performed with iScript cDNA Synthesis Kit (Bio-Rad). qRT-PCR was performed using 10 μL of SsoFast EvaGreen Supermix (Bio-Rad), 0.8 μL of primer (10 μM), and 1 μL of cDNA for each reaction, and the plate was run on a Bio-Rad CFX96 real-time PCR detection system with the following protocol: enzyme activation at 95 °C for 30 s, 39 cycles of denaturation at 95 °C for 5 s, and annealing/extension at 57 °C for 5 s and a melt curve of 65–95 °C in 0.5-°C increments for 5 s. Analysis was performed with the ΔΔCT method using β-actin as a calibrator gene (2). Primer sequences are available elsewhere (1).

Gi-DREADD. On binding to the exogenous ligand CNO, the mutated G_i-coupled receptor Gi-DREADD (also called HM4Di, or Gi) leads to the activation of G protein-gated inwardly rectifying potassium channels (GIRK), hyperpolarization of the expressing cells, and neuronal silencing (3). All surgeries were performed under aseptic conditions and with stereotaxic guidance. Mice were anesthetized using 1–2% isoflurane. All coordinates are relative to bregma in millimeters and defined according to the Paxinos sterotaxic atlas (4). Mice received bilateral injections of AAV_5 virus (titer, 1–5 × 10^{12}). All mice received bilateral

0.3-μL injections of purified AAV_5 (titer, 1–5 × 10^{12}), at a rate of 0.05 μL/min in the BLA (stereotaxic coordinates: −1.34 AP, ±3.35 mm ML, −3.9 mm DV) expressing Gi-DREADD-IRES-mCitrine, or eYFP only, under the CaMKIIα promoter. Injection was done using a beveled 33-gauge microinjection needle facing the posterolateral side to restrict the viral infusion to the BLA. A 10-μL microsyringe (nanofil; WPI) was used to deliver AAV solution using a microsyringe pump (Wiretrol Drummond) and a microinjector (53311; Quintessential Stereotaxic Injector). After the completion of injection, the syringe/needle was left in place for an additional 5 min to allow for virus diffusion, and then slowly withdrawn. The virus was allowed to express for 3 wk before starting the experiment. The Gi-DREADD–activating drug CNO (C0832; Sigma-Aldrich) was diluted in 0.9% sterile saline (Aqualite Systems) and 30 min before the RFS, mice were injected i.p. with 2.5 mg/kg of CNO to both the eYFP controls and Gi-DREADD expressing mice (Fig. S2*A*). Given the pharmacokinetics of CNO as measured in humans, and adjusting for the higher metabolic rate of the mouse by Kleiber's Law, we calculated that this dosage would result in a peak brain tissue concentration of ∼12 mM (Table S1), above the concentrations shown to produce potent neuronal inhibition in slice preparations (3, 5). The eYFP-CON and Gi-CON groups showed some similar results in immunohistochemical and Western blot quantifications and behavioral performance, and thus were pooled into a single group.

Stereotaxic ChR2 Injection and Optical Fiber Placement. Surgeries were performed as before. Transduction of BLA glutamatergic projection neurons was achieved using an adeno-associated virus (AAV_5) vector carrying hChR2(H134R)-eYFP or control virus carrying eYFP only, driven by the CaMKIIα promoter (viruses provided by K. Deisseroth; maps and clones available at web.stanford.edu/group/dlab/optogenetics/). Virus delivery into the BLA was done in the same manner as for the Gi-DREADD–injected mice, with the addition of the bilateral implantation of self-assembled implantable optical fibers. The protocol from the Synthetic Neurobiology Group website (syntheticneurobiology.org/protocols/protocoldetail/35/9) was used to build these, with the only difference being the use of metal ferrules with an internal diameter of 330 μm (Precision Fiber Products) and 300-μm, 0.37 NA fiber optics (Thorlab).

For the ChR2 cell body mice, the implants were placed 0.5 mm dorsal to the BLA (stereotaxic coordinates: −1.34 mm AP, ±3.35 mm ML, and −3.4 mm DV). For the ChR2 terminal experiments, implants were placed 0.5 mm dorsal to the hippocampal CA3 in either the dorsal or ventral hippocampal subregion (stereotaxic coordinates: −2.18 mm AP, ±2.67 mm ML, and −1.37 mm DV or −3.48 AP, ±3.00 mm ML, and −2.80 mm DV, respectively). One layer of adhesive cement (C&B Metabond; Parkell), followed by cranioplastic cement (Dental Cement; Stoelting), were used to secure the implantable optical fibers to the skull. Animals were kept on a heating pad until recovery from anesthesia. Virus was allowed to express for 3 wk for the cell body experiments or 6 wk for the terminal experiments before the laser stimulation paradigms. Correct placement of the optical fiber was verified for each implanted mouse (Fig. S3*G* for the ChR2 cell body experiments; data not shown for the BLA terminal experiments).

Optogenetic Stimulation. For optogenetic stimulation, a fiber optic cable was used to connect a 473-nm laser diode (OEM Laser Systems) through an FC/PC adapter to a rotatory joint (Doric Lenses) mounted inside the fear-conditioning chamber. Laser output was controlled using a Master-8 pulse stimulator (AMPI) to deliver light trains at a 20-Hz, 10-ms pulse width of 473-nm light. Specificity of the stimulation was dependent on fiber optic implant location, and was histologically confirmed in all cases.

The skull-mounted optical fibers were plugged into a branching fiber optic patch cord (Doric Lenses) to split the laser output, providing bilateral light delivery. This patch cord was connected to the external fiber optic cable through the rotary joint inside the fear-conditioning chamber. For the BLA cell body experiment, mice received the laser stimulation for 2 s at a laser intensity of 3–5 mW (∼57 mW/mm^2 at the tip of the fiber). This stimulation was repeated 10 times over a 20-min period at random intervals, once daily for 8 consecutive days. For the BLA hippocampal terminal experiments, mice received the laser stimulation for 20 s at 7–8 mW (∼106 mW/ mm^2 at the tip of the fiber), repeated 10 times during a 20-min session at random intervals and repeated once daily for 8 d.

Corticosterone Assays. After the third session of optogenetic stimulation of BLA terminals, five drops of blood were collected from mice by facial vein puncture using a 5-mm Goldenrod Animal Lancet (MEDIpoint). Samples were kept on ice and heparinized with 10 μL of 1,000 U/mL heparin. Samples were centrifuged at 2,300 × *g* for 10 min at 4 °C, after which the plasma was removed and frozen for later use. A corticosterone ELISA kit (Enzo Life Sciences) was used to measure the concentrations of these samples. The provided steroid displacement reagent was mixed with assay buffer, and this mixture was used to dilute the serum samples to the suggested ratio of 1:50, such that 2.5 parts of steroid displacement reagent were present for every 97.5 parts of undiluted sample. The remainder of the protocol was conducted in accordance with the manufacturer's instructions. Absorbance at 405 nm was read using a multiplate reader (EnSpire; PerkinElmer), blanked to blank wells. Concentration was calculated from the standard curve provided by standard concentration in each plate.

Generation of Δp35 Knock-In Mice. The detailed protocol for production of the Δp35 KI mice has been described previously (6). Δp35 mice were bred for eight generations with Swiss Webster mice to transfer the Δp35 mice under the stress-sensitive Swiss Webster genetic background.

Statistics. Statistical analyses were performed using GraphPad Prism 5. One-way ANOVA followed by Tukey's post hoc test or the one-tailed Student *t* test was used unless specified otherwise. The novel object and novel location recognition tasks were performed using one-sample *t* tests, with the discrimination index applied to assess whether preference for an object was significantly above chance (i.e., mean discrimination ratio >0.5). These one-sample *t* tests were one-tailed, because the only issue was whether scores were above chance. To measure the effect of the Gi-DREADD treatment on BLA neuron excitability, evoked action potentials were quantified and fitted by linear regression, and statistics were calculated using the F test on the slopes. All data are presented as mean ± SEM. Statistical significance was set at $P \leq 0.05$.

1. Gräff J, et al. (2012) An epigenetic blockade of cognitive functions in the neurodegenerating brain. *Nature* 483(7388):222–226.
2. Livak KJ, Schmittgen TD (2001) Analysis of relative gene expression data using real-time quantitative PCR and the 2(-Delta Delta C(T)) method. *Methods* 25(4):402–408.
3. Armbruster BN, Li X, Pausch MH, Herlitze S, Roth BL (2007) Evolving the lock to fit the key to create a family of G protein-coupled receptors potently activated by an inert ligand. *Proc Natl Acad Sci USA* 104(12):5163–5168.
4. Paxinos G, Franklin KBJ (2001) *The Mouse Brain in Stereotaxic Coordinates* (Academic, New York), 2nd ed.
5. Ray RS, et al. (2011) Impaired respiratory and body temperature control upon acute serotonergic neuron inhibition. *Science* 333(6042):637–642.
6. Seo J, et al. (2014) Activity-dependent p25 generation regulates synaptic plasticity and Aβ-induced cognitive impairment. *Cell* 157(2):486–498.

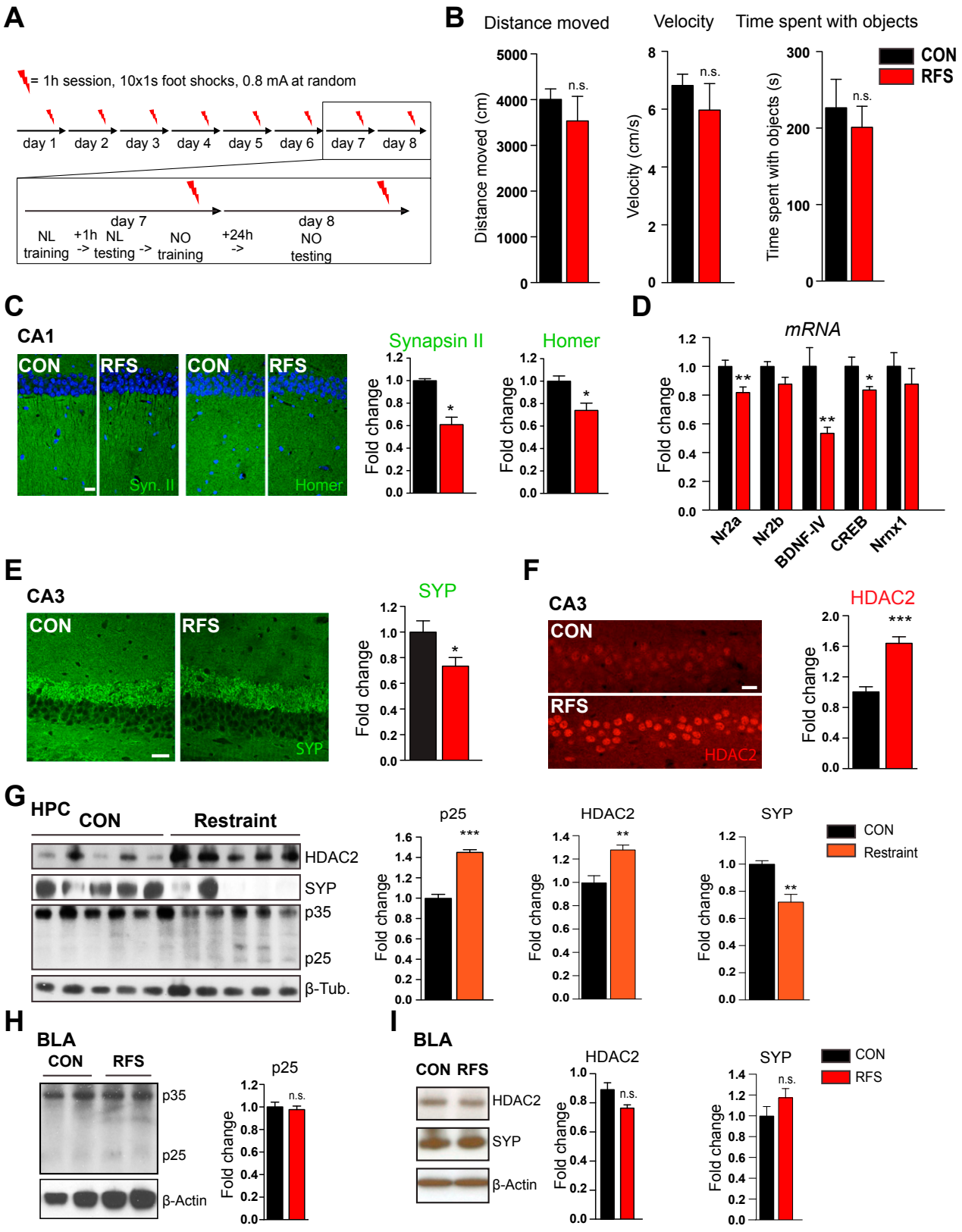

Fig. S1. RFS-treated mice have normal locomotor and object exploration behavior. Restraint stress induces similar hippocampal molecular changes as those seen after RFS. The BLA did not show the molecular changes seen in the hippocampus after repeated stress. (*A*) RFS paradigm and timing of the novel object recognition (NO) and location recognition (NL) tasks (schematic). (*B*) Distance moved, velocity, and total exploration time in the novel object and novel location recognition tasks (unpaired *t* test, $n = 8$ per group). (*C*) Representative immunohistochemical images in dorsal hippocampal CA1 subregion and quantitative analysis of the effect of repeated stress on the expression levels of Synapsin II and Homer (HDAC2 in red; Synaptophysin, Synapsin II, and Homer in green; DAPI

Legend continued on following page

in blue) (unpaired *t* test, $n = 4$ per group). (*D*) qRT-PCR results of the effect of stress on the mRNA level of some known HDAC2 targets. The mRNA levels of these genes were significantly decreased in RFS-treated animals compared with controls. Other HDAC2 targets, such as NR2B and Neurexin, trended toward a decrease in the hippocampus of RFS-treated animals, but did not reach significance (unpaired *t* test, $n = 7$ per group). (*E* and *F*) Representative images and quantification of Synaptophysin (*E*) and HDAC2 (*F*) expression levels in the hippocampal CA3 subregion after RFS (unpaired *t* test, $n = 3$ per group) (Synaptophysin in green; HDAC2 in red). (*G*) Representative Western blot images and quantification of HDAC2, Synaptophysin, and p25 expression levels from control and restraint mice whole hippocampus lysates (unpaired *t* test, $n = 5$ per group). (*H* and *I*) Representative Western blot images and quantification of the effect of RFS on p25 (*H*), HDAC2, and Synaptophysin (*I*) levels in the BLA (unpaired *t* test, $n = 5$ per group). Values are mean ± SEM. n.s., nonsignificant; $P > 0.05$; $^{*}P \leq 0.05$; $^{**}P \leq 0.01$; $^{***}P \leq 0.001$, unpaired *t* test. (Scale bars: 20 μm in *C* and 50 μm in *E* and *F*.)

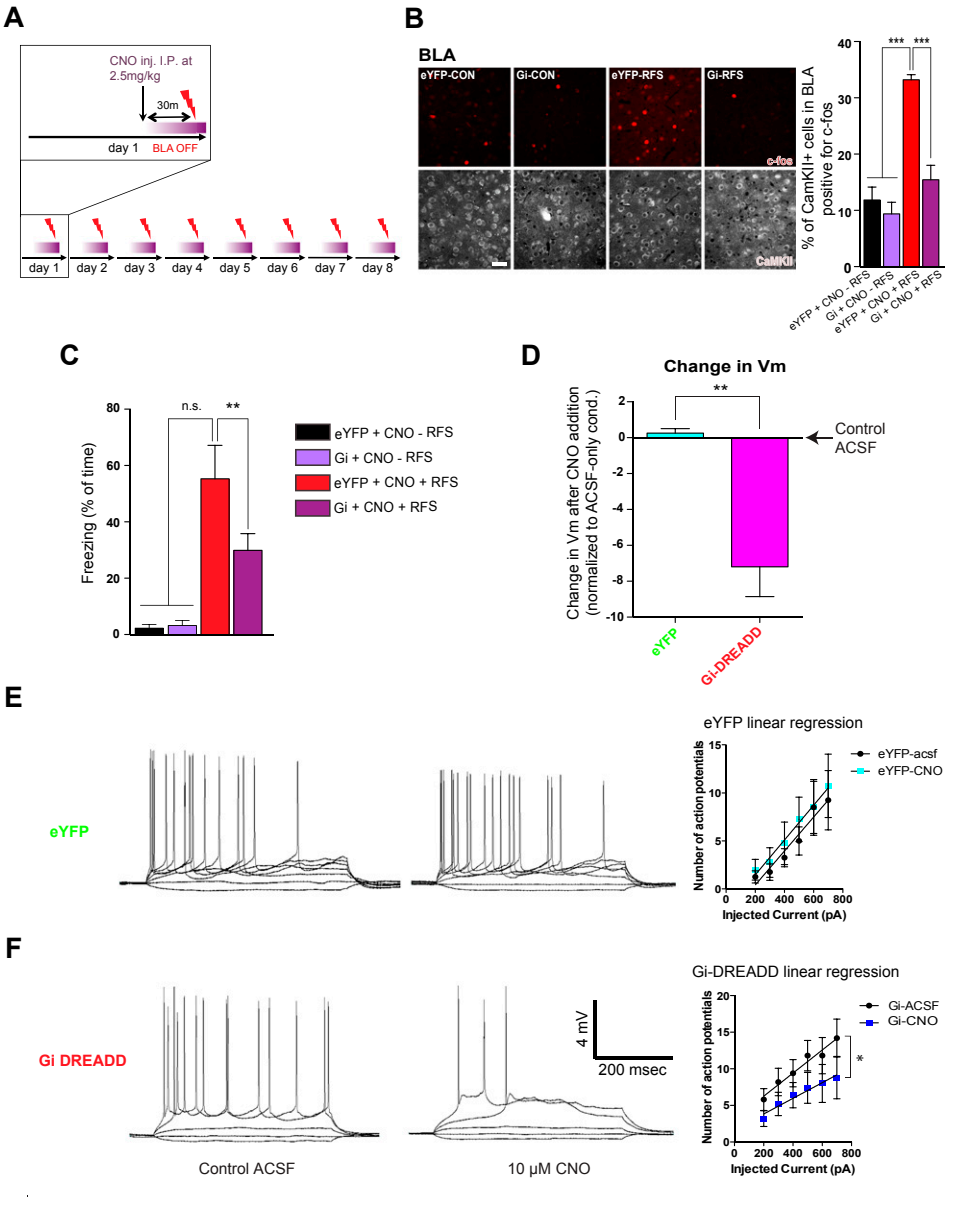

Fig. S2. Gi-DREADD efficiently silences the BLA during RFS. (*A*) Experimental protocol used to mediate DREADD-induced BLA inhibition during RFS. (*B*) Representative images and quantification of the effect of the Gi-DREADD BLA inhibition on the number of c-fos/CAMKII double-positive cells in the BLA (one-way ANOVA with Tukey's post hoc test; $n = 4$ per group) (c-fos in red; CaMKII in white). (*C*) Automated quantification of the effect of Gi-DREADD BLA inhibition on behavioral freezing levels during the interfoot shock intervals in the RFS paradigm (one-way ANOVA with Tukey's post hoc analysis, $n = 6$ mice per group). (*D*) Hyperpolarization of membrane potential after 10 μM CNO perfusion in Gi-DREADD–expressing BLA neurons compared to control eYFP-expressing neurons (unpaired *t* test, $n = 5$ cells from 4 slices prepared from 3 different animals per group). (*E* and *F*) Cellular excitability as approximated by the number of action potentials at multiple current injections before and after bath application of 10 μM CNO to BLA brain slices from mice transduced with the eYFP control (*E*) or Gi-DREADD (*F*) virus ($P = 0.02857$, F-test on slopes, $n = 5$ cells from 4 slices prepared from 3 different animals per group). Values are mean ± SEM. n.s., nonsignificant; $P > 0.05$; $^{*}P \leq 0.05$; $^{**}P \leq 0.01$; $^{***}P \leq 0.001$, unpaired *t* test. (Scale bar: 50 μm.)

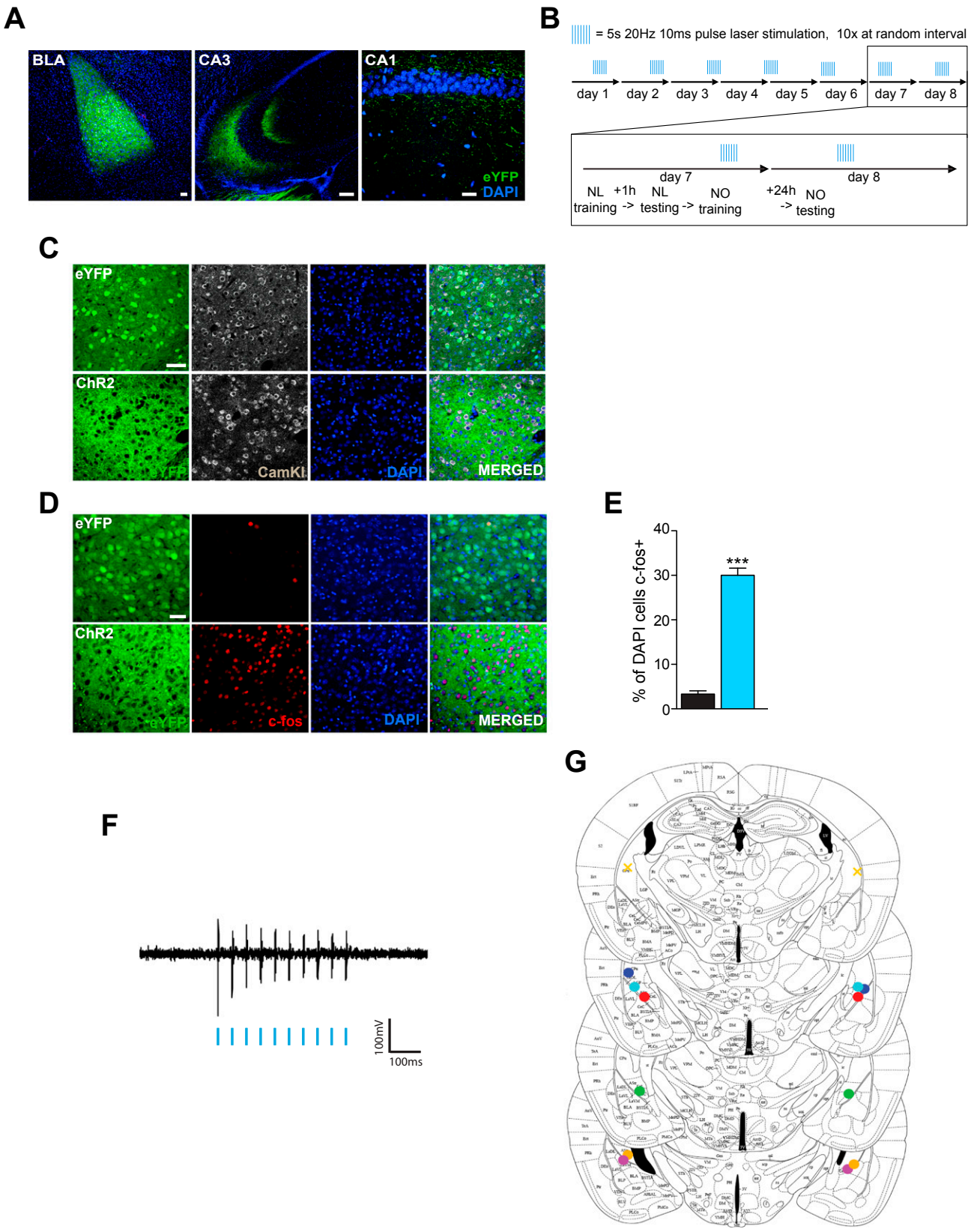

Fig. S3. Efficient targeting allows for precise spatiotemporal control of glutamatergic BLA neurons. (*A*) Immunohistochemical images of a coronal section containing the BLA (*Left*), dorsal hippocampal CA3 (*Center*), and dorsal hippocampal CA1 (*Right*) from a ChR2-mouse (eYFP-positive cell bodies or axon terminals in green; DAPI in blue). (*B*) Laser illumination protocol used for ChR2-mediated BLA photostimulation and timing for the novel object (NO) and novel location (NL) recognition tasks (schematic). (*C*) Representative immunohistochemical images of the expression pattern of eYFP and ChR2-eYFP in CaMKII-positive cells, in the BLA of eYFP or ChR2 BLA cell body photostimulated mice (eYFP in green; CaMKII in white; DAPI in blue).

Legend continued on following page

(*D* and *E*) Representative images and quantification of the number of DAPI/c-fos double-positive cells in the BLA from ChR2 mice compared with eYFP mice (unpaired *t* test, $n = 5$ per group) (eYFP in green; c-fos in red; DAPI in blue). (*F*) Representative single-unit recording trace of a ChR2-eYFP positive neuron illuminated with blue light (single pulse of light represented as a blue bar). (*G*) Placement of fiber optic implants was verified for each mouse and is represented with one color code per animal. Circles represent animals with proper fiber placement, and crosses represent animals in which fibers were not located 0.5 mm dorsal to the BLA and were excluded from the study. (Scale bars: 50 μm in *A*, *Left* and *Middle*, and *C*; and 20 μm in *A*, *Right*, and *D*.)

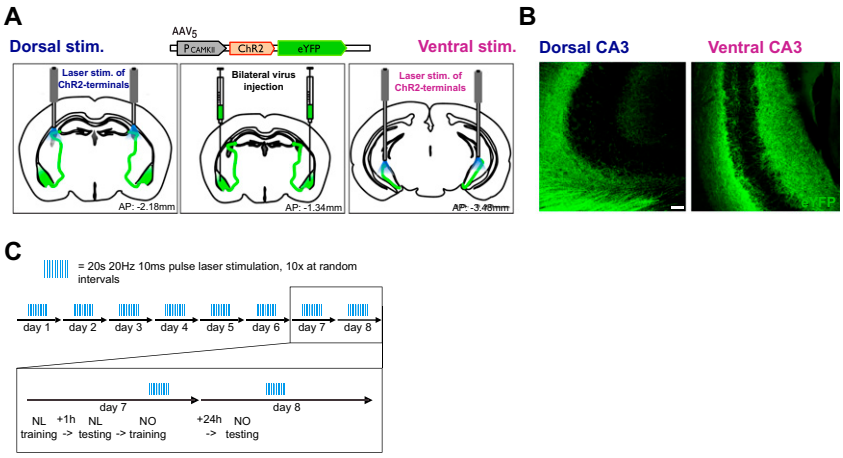

Fig. S4. Protocol of BLA terminals stimulation in the hippocampus and representative images of eYFP-expressing BLA fibers at the sites of stimulation. (*A*) Schematic of the protocol for virus injection and fiber optic placement for the dorsal and ventral hippocampus stimulation. (*B*) Representative maximum intensity projections from 15 images (spanning 15 μm) from a coronal section containing eYFP-positive BLA terminals in the dorsal and ventral CA3 from a ChR2 mouse (eYFP-positive terminals in green). (*C*) Laser illumination protocol used for BLA terminal photostimulation (schematic). NO, novel object recognition; NL, novel location recognition. (Scale bar: 20 μm.)

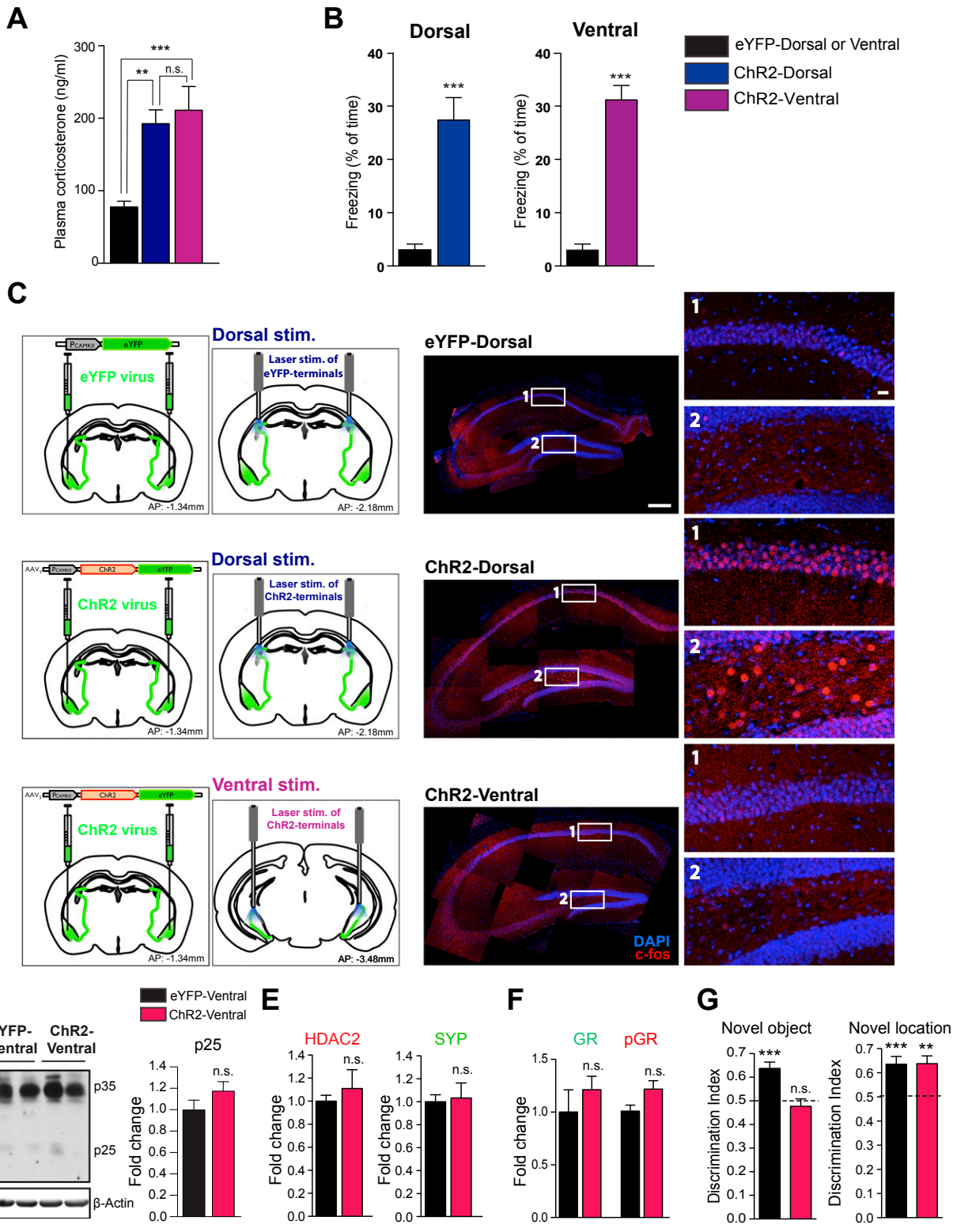

Fig. S5. Activity of the dorsal hippocampus is increased by terminal photostimulation of BLA projections in the dorsal, but not the ventral, hippocampus and BLA terminals after stimulation in the ventral hippocampus does not increase p25 generation in the dorsal hippocampus. (*A* and *B*) Effect of ChR2-mediated BLA terminal photostimulation in either the dorsal or ventral hippocampus on plasma corticosterone levels (*A*) and on freezing behavior during the laser ON periods, automated counting (*B*) (unpaired *t* test) (*A*, $n = 4$ mice per group; *B*, $n = 4$ and 6 animals each). (*C*) Schematic for each of the experimental groups and representative images of the c-fos signal in the dorsal hippocampus of mice receiving illumination of BLA terminals in either the dorsal hippocampus (*Top*, eYFP mouse; *Middle*, ChR2 mouse), or the ventral hippocampus (*Bottom*, ChR2 mouse) (c-fos in red; DAPI in blue). (*D*) Effect of BLA terminal photostimulation in the ventral hippocampus on p25 generation in the dorsal hippocampus (unpaired *t* test, $n = 5$ per group). (*E*–*G*) Effect of terminal photostimulation of BLA fibers in the ventral hippocampus on the expression level of HDAC2 and Snaptophysin (*E*), GR and pGR (*F*) in the dorsal CA1 hippocampal subregion, and on the novel object and novel location recognition tasks (*G*). n.s., nonsignificant; $P > 0.05$; ***$P \leq 0.001$. Values are mean ± SEM. (Scale bars: *C*, *Left*, 100 μm; *C*, *Right*, 20 μm.)

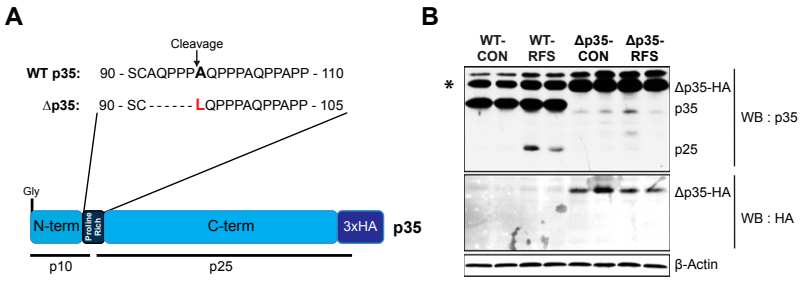

Fig. S6. p25 generation following stress is blocked in the Δp35KI mice. (*A*) Mutations in the calpain cleavage site of p35 produce an uncleavable form of p35 in the Δp35KI mice (schematic). (*B*) (*Upper*) Effect of the Δp35KI genotype on p25 generation following RFS, measured in hippocampal lysates from Δp35KI mice and control littermates. (*Lower*) Expression of Δp35 was confirmed in the Δp35KI hippocampus by immunoblotting with an anti-HA antibody. *Nonspecific background band visible in the WT lanes that comigrates with Δp35-HA.

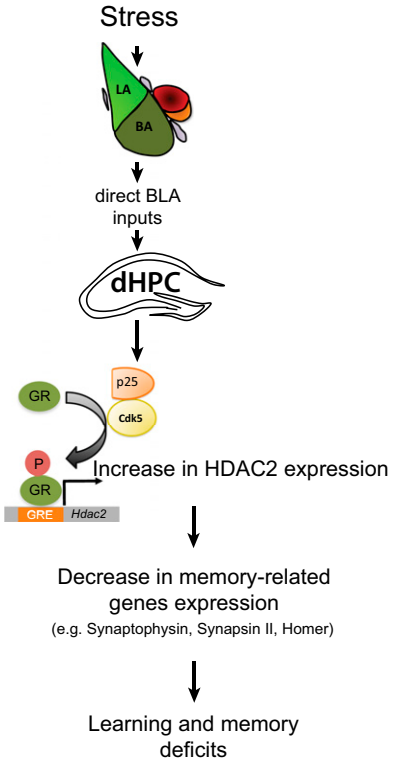

Fig. S7. Model of the generation of p25 by neural circuit activity after repeated stress to suppress learning and memory. We propose that BLA hyperactivation after repeated stress leads to an increase in its glutamatergic input on the dorsal hippocampus. Activation of this neural circuit triggers a molecular pathway previously reported to be involved in AD-associated neurotoxicity. This pathway consists of generation of p25; increases in GR, pGR, and HDAC2 expression levels; and down-regulation of memory-related genes, leading to a deficit in hippocampus-dependent learning and memory.

Table S1. Pharmacokinetics of CNO

Pharmacokinetic property of CNO	Value	Reference/derivation
Half-life ($t_{1/2}$) (human)	8.6 h	1
Clearance (Cl) (human)	45.3 L/h (40 kg human)	2
Volume of distribution (V_D) (human)	562 L (40 kg human)	$V_{-D} = (Cl \cdot t_{1/2})/\ln 2$
Volume of distribution (V_D) (mouse)	0.2409 L (30 g mouse)	α body mass
Clearance (mouse)	0.1352 L/hr (30 g mouse)	Kleiber's Law: $q0 \sim M^{3/4}$
Partition coefficient	14.05	V_{-D}/total body water
Effective concentration	1–10 μM	3, 4

1. Guitton C, Kinowski J-M, Abbar M, Chabrand P, Bressolle F (1999) Clozapine and metabolite concentrations during treatment of patients with chronic schizophrenia. *J Clin Pharmacol* 39(7):721–728.
2. Chang WH, et al. (1998) Reversible metabolism of clozapine and clozapine N-oxide in schizophrenic patients. *Prog Neuropsychopharmacol Biol Psychiatry* 22(5):723–739.
3. Ray RS, et al. (2011) Impaired respiratory and body temperature control upon acute serotonergic neuron inhibition. *Science* 333(6042):637–642.
4. Armbruster BN, Li X, Pausch MH, Herlitze S, Roth BL (2007) Evolving the lock to fit the key to create a family of G protein-coupled receptors potently activated by an inert ligand. *Proc Natl Acad Sci USA* 104(12):5163–5168.